Design and Optimization of Dual Band Circular Polarization Selective Structures

Lundgren, Johan; Ericsson, Andreas; Sjöberg, Daniel

2017

CODEN:LUTEDX/(TEAT-7257)/1-21/(2017)

Design and Optimization of Dual Band Circular Polarization Selective Structures

Johan Lundgren, Andreas Ericsson and Daniel Sjöberg

Electromagnetic Theory
Department of Electrical and Information Technology
Lund University
Sweden

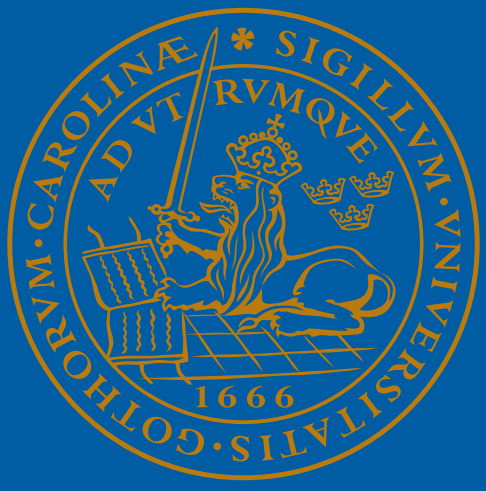

(TEAT-7257)/1-21/(2017): J. Lundgren, A.Ericsson, D. Sjöberg, Dual Band Circular Polarization Selective Structures

Johan Lundgren
johan.lundgren@eit.lth.se

Andreas Ericsson
andreas.ericsson@eit.lth.se

Daniel Sjöberg
daniel.sjoberg@eit.lth.se

Department of Electrical and Information Technology
Electromagnetic Theory
Lund University
P.O. Box 118
SE-221 00 Lund
Sweden

This is an author produced preprint version of the paper:

J. Lundgren, A. Ericsson, and D. Sjöberg. "Design and Optimization of Dual Band Circular Polarization Selective Structures". *Transactions on Antennas and Propagation* (2017), under review.

Homepage `http://www.eit.lth.se/teat`

Editor: Mats Gustafsson

Abstract

We present a non-resonant, dual band circular polarization selective structure (CPSS) for satellite communication applications in the K- and K_a-band. The structure consists of multiple layers of cascaded anisotropic sheets, with printed meander lines, separated by low permittivity spacers. It reflects right hand circular polarization and transmits left hand circular polarization in the lower frequency band. In the upper frequency band the opposite polarization selectivity is achieved. The theory of dual band circular polarization selectivity from cascaded anisotropic sheets is presented, and it is concluded that the separation between the frequency bands of operation is governed by the relative rotation between subsequent layers. An optimization routine for synthesizing dual band CPSSs from predefined design requirements is introduced, where a number of different optimization algorithms are utilized. A simulated design is presented which fulfills the strict design requirements of insertion loss and return loss less than 0.5 dB, and axial ratio less than 0.78 dB, in the frequency bands 17.7–20.2 GHz and 27.5–30.0 GHz. A prototype of the optimized design has been fabricated and characterized experimentally, both in transmission and reflection, and good agreement is observed between simulated and experimental results. This type of structure is a potential candidate for implementation in dual band multiple spot beam systems utilizing frequency and polarization reuse schemes.

1 Introduction

Key components in today's interconnected world are communication satellites positioned in crowded orbits [7]. In order to utilize the available satellite aperture in a more efficient manner, frequency and polarization reuse schemes can be utilized [15]. By using dual band satellite communication (SATCOM) systems these satellites can be improved by reducing the number of reflectors needed by a factor of two [2]. An example of such a system was recently presented in [18], where a dual band polarizing surface converting linear polarization (LP) to circular polarization (CP) was used as a reflector in the K_u-band. Alternative solutions to this system can be achieved using dual band circular polarization selective structures (CPSSs), either as diplexers or reflectors. A dual band CPSS will for the lower frequency band reflect one handedness of CP while transmitting the orthogonal circular polarization, and do the converse for the higher frequency band [12].

In the last century, many different CPSS designs have been presented with various performance levels [1, 8, 13, 14, 17, 19, 21, 22, 23]. An overview of the CPSSs presented up to date is presented in [5], where these structures are evaluated with respect to relevant performance requirements. Recently, a high performing, wide band CPSS concept based on non-resonant elements was presented [3, 4, 5, 16]. These designs all consist of multiple sheets of meander lines stacked and rotated after one another. Each layer is perceived as an effective capacitance/inductance in linear polarization by incident waves. A shortcoming of previously presented CPSSs is that the design and optimization have been carried out to obtain operation in a

single frequency band. In the same manner as in a frequency selective structure, higher order resonances can be observed in a CPSS. However, the frequency separation between these resonances is generally much larger than what is desirable, and to optimize a CPSS for dual band operation is a challenging task.

To this end, we present a design procedure for dual band CPSSs consisting of multiple layers of anisotropic sheets. In the same manner as in [3, 4, 5, 16], subwavelength meander lines are used to achieve a strong anisotropic response in the sheets. The frequency bands of interest in this work are the SATCOM downlink band $17.7 - 20.2\,\mathrm{GHz}$ and the uplink band $27.5 - 30.0\,\mathrm{GHz}$, located in the K- and $\mathrm{K_a}$-bands. To the authors' knowledge, this is the first time a dual band CPSS is presented with performance levels applicable to real world configurations.

The paper is organized as follows: in Section 2 the theory of scattering in circular polarization from anisotropic sheets is presented. It is shown that the optimal number of layers of a CPSS can be found in order to achieve CP selectivity in multiple frequency bands, and to reduce the cross polarization scattering. A detailed optimization procedure is introduced in Section 3, where a dual band CPSS is designed based on predefined performance requirements. Simulation results of the optimized design are presented in Section 4. A prototype was manufactured and the details of this test panel are presented in Section 5, and experimental results of this structure are evaluated in Section 6. Finally, some concluding remarks are presented in Section 7.

2 Theory - dual band circular polarization selectivity from linear elements

The scattering matrix in circular polarization of a system with two ports, located on each side of the sample, is

$$\mathbf{S}^{\mathrm{CP}} = \begin{pmatrix} S_{11}^{\mathrm{RR}} & S_{11}^{\mathrm{RL}} & S_{12}^{\mathrm{RR}} & S_{12}^{\mathrm{RL}} \\ S_{11}^{\mathrm{LR}} & S_{11}^{\mathrm{LL}} & S_{12}^{\mathrm{LR}} & S_{12}^{\mathrm{LL}} \\ S_{21}^{\mathrm{RR}} & S_{21}^{\mathrm{RL}} & S_{22}^{\mathrm{RR}} & S_{22}^{\mathrm{RL}} \\ S_{21}^{\mathrm{LR}} & S_{21}^{\mathrm{LL}} & S_{22}^{\mathrm{LR}} & S_{22}^{\mathrm{LL}} \end{pmatrix}, \tag{2.1}$$

where the superscript R stands for right hand circular polarization (RHCP) and similarly L stands for left hand circular polarization (LHCP). The subscripts 1 and 2 indicate the number of the receiving and transmitting port. Throughout this work, the time convention $\mathrm{e}^{\mathrm{j}\omega t}$ is used, and for the definition of circular polarization the IEEE definition is followed [6]. An ideal right hand circular polarization selective structure (RHCPSS) should reflect RHCP waves and transmit LHCP waves, while maintaining the polarization state of the signals, and is described by

$$\mathbf{S}^{\mathrm{RHCPSS}} = \begin{pmatrix} \mathrm{e}^{-\mathrm{j}\phi_{\mathrm{r}}} & 0 & 0 & 0 \\ 0 & 0 & 0 & \mathrm{e}^{-\mathrm{j}\phi_{\mathrm{t}}} \\ 0 & 0 & \mathrm{e}^{-\mathrm{j}\phi_{\mathrm{r}}} & 0 \\ 0 & \mathrm{e}^{-\mathrm{j}\phi_{\mathrm{t}}} & 0 & 0 \end{pmatrix}, \tag{2.2}$$

where ϕ_t and ϕ_r are the phases of the transmission and reflection coefficients, respectively. Similarly, an ideal left hand circular polarization selective structure (LHCPSS) is described by

$$\mathbf{S}^{\mathrm{LHCPSS}} = \begin{pmatrix} 0 & 0 & \mathrm{e}^{-\mathrm{j}\phi_\mathrm{t}} & 0 \\ 0 & \mathrm{e}^{-\mathrm{j}\phi_\mathrm{r}} & 0 & 0 \\ \mathrm{e}^{-\mathrm{j}\phi_\mathrm{t}} & 0 & 0 & 0 \\ 0 & 0 & 0 & \mathrm{e}^{-\mathrm{j}\phi_\mathrm{r}} \end{pmatrix}. \tag{2.3}$$

The scattering matrix of an ideal dual band CPSS will be represented by either (2.2) or (2.3) for a certain frequency f_1 and the other for frequency f_2.

A layer of infinite extent in the plane perpendicular to the direction of propagation, and of infinitesimal thickness, can be described by the reflection coefficients (r_x, r_y), and the transmission coefficients $(t_x = 1 + r_x, t_y = 1 + r_y)$ in LP. It can also be represented by a scattering matrix in CP [12], where the CP scattering matrix for the linear element is given by

$$\begin{aligned} \mathbf{S}^{\mathrm{CP}}_{\mathrm{Linear}} = \frac{r_x + r_y}{2} \begin{pmatrix} 0 & 1 & 1 & 0 \\ 1 & 0 & 0 & 1 \\ 1 & 0 & 0 & 1 \\ 0 & 1 & 1 & 0 \end{pmatrix} + \begin{pmatrix} 0 & 0 & 1 & 0 \\ 0 & 0 & 0 & 1 \\ 1 & 0 & 0 & 0 \\ 0 & 1 & 0 & 0 \end{pmatrix} \\ + \frac{r_x - r_y}{2} \begin{pmatrix} \mathrm{e}^{-2\mathrm{j}\theta_i} & 0 & 0 & \mathrm{e}^{-2\mathrm{j}\theta_i} \\ 0 & \mathrm{e}^{2\mathrm{j}\theta_i} & \mathrm{e}^{2\mathrm{j}\theta_i} & 0 \\ 0 & \mathrm{e}^{2\mathrm{j}\theta_i} & \mathrm{e}^{2\mathrm{j}\theta_i} & 0 \\ \mathrm{e}^{-2\mathrm{j}\theta_i} & 0 & 0 & \mathrm{e}^{-2\mathrm{j}\theta_i} \end{pmatrix}, \end{aligned} \tag{2.4}$$

where θ_i is the rotation of the element in the plane. A single layer cannot be reduced to any of the ideal cases (2.2) or (2.3), but these properties can be achieved by stacking several layers each rotated with respect to the previous layer and separated a distance d. Assuming $r_y = 0$, $r_x = r$ and using the Born approximation treating the elements as weak scatterers [10], the scattering matrix for multiple layers of linear elements can be shown to be

$$\begin{aligned} \mathbf{S}_{\mathrm{Linear}} = \mathrm{e}^{-\mathrm{j}kd} \begin{pmatrix} 0 & 0 & 1 & 0 \\ 0 & 0 & 0 & 1 \\ 1 & 0 & 0 & 0 \\ 0 & 1 & 0 & 0 \end{pmatrix} \\ + \sum_{n=1}^{N} \frac{r}{2} \begin{pmatrix} \mathrm{e}^{-2\mathrm{j}(kz_n+\theta_n)} & \mathrm{e}^{-\mathrm{j}kz_n} & \mathrm{e}^{-\mathrm{j}kd} & \mathrm{e}^{-\mathrm{j}(kd+2\theta_n)} \\ \mathrm{e}^{-2\mathrm{j}kz_n} & \mathrm{e}^{-2\mathrm{j}(kz_n-\theta_n)} & \mathrm{e}^{-\mathrm{j}(kd-2\theta_n)} & \mathrm{e}^{-\mathrm{j}kd} \\ \mathrm{e}^{-\mathrm{j}kd} & \mathrm{e}^{-\mathrm{j}(kd-2\theta_n)} & \mathrm{e}^{-2\mathrm{j}(kz_n+\theta_n)} & \mathrm{e}^{-2\mathrm{j}kz_n} \\ \mathrm{e}^{-\mathrm{j}(kd+2\theta_n)} & \mathrm{e}^{-\mathrm{j}kd} & \mathrm{e}^{-2\mathrm{j}kz_n} & \mathrm{e}^{-2\mathrm{j}(kz_n-\theta_n)} \end{pmatrix}, \end{aligned} \tag{2.5}$$

where N is the number of layers, z_n is the position of the n:th layer and θ_n is the rotation of the n:th layer. With equidistant placement and the same rotation between each layer the relevant reflection parameters in the scattering matrix can

be described by

$$S_{11}^{\mathrm{RR}} = \frac{r}{2}\sum_{n=1}^{N} \mathrm{e}^{-\mathrm{j}2n(kd+\theta)}, \tag{2.6}$$

$$S_{11}^{\mathrm{LL}} = \frac{r}{2}\sum_{n=1}^{N} \mathrm{e}^{-\mathrm{j}2n(kd-\theta)}, \tag{2.7}$$

$$S_{11}^{\mathrm{RL}} = S_{11}^{\mathrm{LR}} = \frac{r}{2}\sum_{n=1}^{N} \mathrm{e}^{-\mathrm{j}2nkd}. \tag{2.8}$$

When the phase distance between two layers equals the relative rotation of the linear elements, $k_1 d = \theta$, (2.7) is maximized and LHCP waves are reflected. If the direction of rotation between the layers is mirrored, *i.e.* $\theta = -k_1 d$, (2.6) is instead maximized and thus the opposite polarization (RHCP) is reflected. Given that either (2.6) or (2.7) is maximized, the number of layers N can be chosen to minimize the reflection of the orthogonal co-polarized component as well as the cross polarization terms (2.8). A detailed derivation of the lowest optimal number of layers (N_{opt}) is presented in [12], where it is concluded that this quantity is given by the smallest denominator of θ/π when this is a rational number. To summarize, if $\theta = -k_1 d < 0$ the structure is an RHCPSS at the frequency f_1, corresponding to the wave number k_1. Another solution is achieved when $k_2 d = \pi + \theta = \pi - k_1 d$. Then (2.7) is maximized and for the previously chosen N_{opt} (2.6) and (2.8) are still minimized. This indicates that the structure is an LHCPSS at the frequency f_2, corresponding to the wave number k_2, and the relation between the two bands is given by,

$$f_2 = \frac{\pi - |\theta|}{|\theta|} f_1. \tag{2.9}$$

A physical explanation of these two solutions, and thus the dual band behavior, is as follows. At a fixed instant in time, an electromagnetic CP wave with frequency f_1 propagating in the z-direction through a multilayered CPSS will have a certain phase distribution as it interacts with each of the anisotropic layers, as in Figure 1. If the polarization of the wave rotates in a certain direction in space as a function of the distance z, and the rotation between each layer of the structure θ matches this rotation, the wave will align with the layers and be reflected. This situation is described by the relation $k_1 d = -\theta$. The orthogonal polarization will be misaligned with each layer and thus will be transmitted. However, if another wave at a different frequency f_2 rotates in the opposite direction in space it would also align with the layers the same way if the change of phase between the layers was $k_2 d = \pi + \theta = \pi - k_1 d$. Thus, dual band CP selectivity is achieved with interchanged reflection and transmission properties in the two bands, and the two reflected waves are illustrated in Figure 1.

The selectivity in transmission is not treated by the theory of weak scattering in (2.5)–(2.8), but can be motivated from a power conservation point of view. The co-polarized transmission amplitude is bounded by $|S_{mn}^{ll}|^2 \leq 1 - |S_{nn}^{ll}|^2 -$

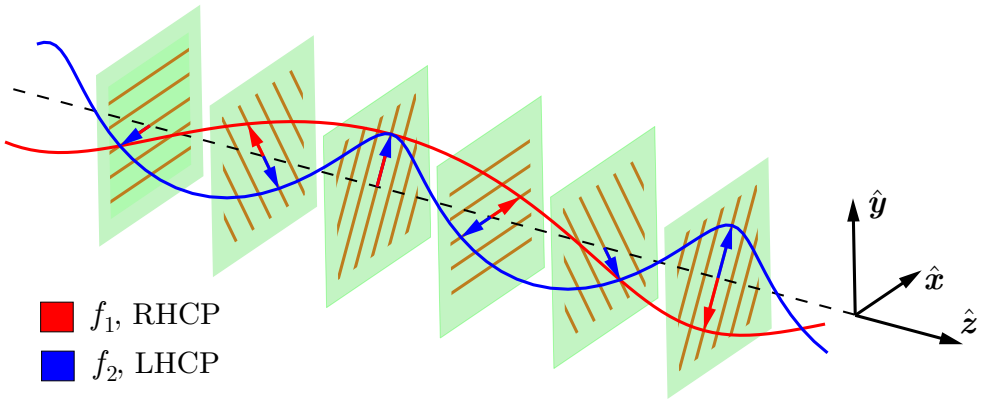

Figure 1: The principle of operation of a dual band CPSS illustrated at a fixed instant in time t, where RHCP waves at frequency f_1 rotate $\theta = -\pi/3$ radians between each layer and LHCP waves at frequency f_2 rotate $\pi + \theta = 2\pi/3$ radians (in the opposite direction).

$|S_{nn}^{kl}|^2 - |S_{mn}^{kl}|^2$, where $m, n \in \{1, 2\}$ are the receiving and transmitting ports, and $k, l \in \{\text{RHCP}, \text{LHCP}\}$ are the polarization state of the received and transmitted waves. If the co-polarized reflection amplitude $|S_{nn}^{ll}|$ is close to one the co-polarized transmission amplitude $|S_{mn}^{ll}|$ will be small. Conversely, if the co-polarized reflection amplitude is weak, the co-polarized transmission amplitude will be strong, provided weak cross-polarization scattering and low losses.

The choice of the rotation angle θ between the CPSS layers will depend on the desired frequency separation of the bands and the optimal number of layers. In Table 1 different feasible values of θ, the corresponding lowest optimal number of layers, and the frequency separation of the two bands are shown. A general pattern that can be observed is that smaller relative rotations result in larger separations between the frequency bands, and vice versa.

For the proposed frequency bands of $17.7 - 20.2\,\text{GHz}$ and $27.5 - 30.0\,\text{GHz}$ a rotation of $\theta = 76.3°$ would be preferable. This is illustrated in Figure 2, where the reflection of a dual band CPSS consisting of 5 equidistantly placed layers of linear elements, each rotated $\theta = 76.3°$ with respect to the previous layer, has been simulated using the expressions (2.6)–(2.8). The cross polarization is not minimized with this number of layers but it is low. However, this choice of θ cannot be implemented in a full wave simulation model as the unit cell construction using periodic boundary conditions is infeasible if the number of layers is larger than three. For such a periodic structure consisting of connected elements, modeled with periodic boundary conditions, the feasible choices of θ are $\{45°, 60°\}$ [12]. To this end, $\theta = 60°$ is used in this work as the frequency separation of the two bands are better suited than that of $\theta = 45°$.

Table 1: The number of layers and for what frequencies the dual band CPSS is operating for a certain rotation between layers.

Rotation - degree / (radian)	$N_{\min}$	f_2
18° / ($\pi/10$)	10	$9f_1$
20° / ($\pi/9$)	9	$8f_1$
22.5° / ($\pi/8$)	8	$7f_1$
24° / ($2\pi/15$)	15	$6.5f_1$
30° / ($\pi/6$)	6	$5f_1$
36° / ($\pi/5$)	5	$4f_1$
40° / ($2\pi/9$)	9	$3.5f_1$
45° / ($\pi/4$)	4	$3f_1$
60°/ ($\pi/3$)	3	$2f_1$
72° / ($2\pi/5$)	5	$1.5f_1$

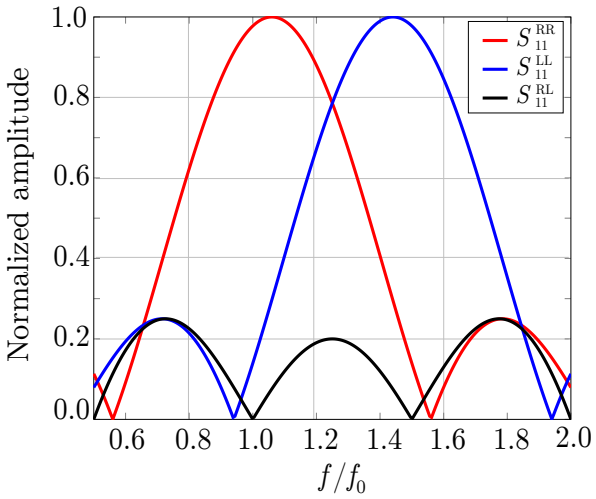

Figure 2: Reflection simulations of a five layer dual band CPSS using the weak scattering approximation. Scattering parameters of normalized magnitude are here presented as a function of normalized frequency.

3 Design and optimization

A multitude of dual band CPSS designs, consisting of different numbers of meander line sheets, were optimized and evaluated in [12]. There it was observed that adding more layers to the structure increases the potential bandwidth of the CPSS, but also increases the design complexity of the structure. It was shown that the wide bandwidth displayed in [5] can be traded for improved dual band performance by relocating the frequency bands of operation closer to each other. The study in [12] provided a starting point for designing and optimizing a dual band CPSS in

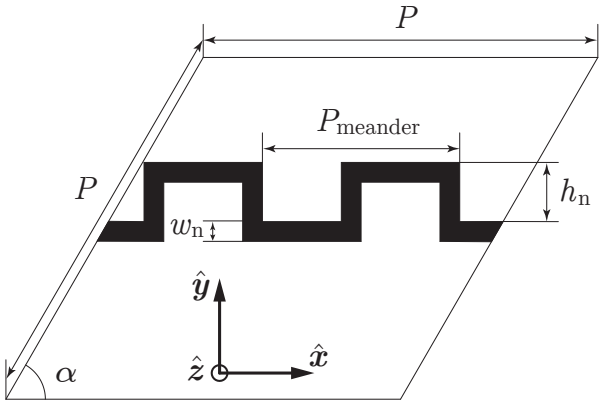

Figure 3: Geometry of a meander line unit cell. The tilt angle of the unit cell α is chosen to be equal to $\theta = 60°$.

this work. As was mentioned in Section 2, the rotation angle $\theta = 60°$ is used and meander lines are utilized as linear elements as they previously have been successfully used to simulate and manufacture a single band wide band CPSS [4, 5]. However, the optimization procedure presented in this section can be used to design dual band CPSS with any kind of elements. Realistic materials were implemented in the simulation model, where copper meander lines were printed on thin substrates, separated by low permittivity spacers and assembled together using thin bonding films. Further details of the materials used are presented in Sections 4–5.

The meander line geometry for a single layer is depicted in Figure 3, where a unit cell is shown and design parameters are introduced to describe the unit cell and the meander line. There are two periods of the meander line in one unit cell to achieve a desired meander line alignment in the infinite structure, see [12] for details. The three dimensional unit cell has the shape of a parallelepiped and the periodicity of the unit cell is shared between all layers. Increasing the number of layers, given $N = aN_{\text{opt}}$ ($a \in \mathbb{N}$), increases control of the polarization purity of reflected and transmitted CP waves. However, in a realistic design increasing the number of layers is problematic as the losses in the materials become more significant and the fabrication of the design becomes more challenging. Moreover, each additional layer of meander lines adds to the dimension of the parameter space, resulting in higher complexity of the optimization problem.

Due to the high number of degrees of freedom in the design, multilayer CPSS are quite complex from an optimization point of view. Thus, symmetry around the center of the structure in the $\hat{\boldsymbol{z}}$-direction is enforced in order to reduce the design complexity. This roughly reduces the dimension of the problem by half. The design parameters used are the width and height of the meander lines, the thickness of each spacer between the layers and the periodicity of the meander lines. For a design with an even number of layers this results in $\frac{3}{2}N + 1$ optimization parameters where N is the number of layers, similarly for a design with an odd number of layers the number of optimization parameters are $\frac{3}{2}(N + 1)$. In this work, six layers were chosen for the design based on a compromise between performance and design complexity.

To evaluate the designs during the optimization process a number of performance parameters are introduced. For a CPSS the relevant properties to examine are the losses in transmission and reflection as well as the purity of the circular polarization in both reflection and transmission for the relevant polarization. These parameters are quantified as insertion loss (IL), return loss (RL) and axial ratio (AR). The definition of these parameters, in dB, is

$$\mathrm{IL} = -20\log 10(|S^{ll}_{mn}|), \qquad m \neq n, \tag{3.1}$$

$$\mathrm{RL} = -20\log 10(|S^{ll}_{nn}|), \tag{3.2}$$

$$\mathrm{AR_t} = 20\log 10\left(\left|\frac{|S^{kl}_{mn}| + |S^{ll}_{mn}|}{|S^{kl}_{mn}| - |S^{ll}_{mn}|}\right|\right), \qquad k \neq l, \;\; m \neq n, \tag{3.3}$$

$$\mathrm{AR_r} = 20\log 10\left(\left|\frac{|S^{kl}_{nn}| + |S^{ll}_{nn}|}{|S^{kl}_{nn}| - |S^{ll}_{nn}|}\right|\right), \qquad k \neq l, \tag{3.4}$$

where, as previously introduced in Section 2, $m, n \in \{1, 2\}$ are the receiving and transmitting ports, and $k, l \in \{\mathrm{RHCP}, \mathrm{LHCP}\}$ are the polarization state of the received and transmitted waves.

The targeted goals to be fulfilled in both frequency bands, are IL and RL less than 0.5 dB for the relevant polarization, and AR less than 0.78 dB. These performance levels were previously introduced in an analogous project involving a single band CPSS [2]. For a dual band CPSS there are in total eight target goals to fulfill, summarized in Table 2. In this project, the structure was designed to reflect RHCP in the lower frequency band and LHCP in the upper frequency band, which could easily be interchanged by mirroring the structure.

From the specified performance parameters and target values a penalty function F is introduced. Finding a suitable design implies minimizing F, which has the general form

$$F = \sum_{n=1}^{2}\sum_{m=1}^{4} c_{n,m} \int_{\Omega_n} |g_{n,m}|^{k_{n,m}} \cdot \mathrm{H}(g_{n,m})\,\mathrm{d}f, \tag{3.5}$$

with

$$g_{n,m}(f) = h_{n,m}(f) - l_{n,m}, \tag{3.6}$$

where index n is for each band, index m is for the performance parameter, $c_{n,m}$ is the weight of each function, $h_{n,m}$ are the performance functions of interest (see Table 2), $l_{n,m}$ are the thresholds under which the integrand is zero, Ω_n is the integration domain specified by the frequency bands, $k_{n,m}$ are exponent weights and H is the Heaviside (or unit step) function.

The penalty function contains several local minima which is problematic for many optimization routines. To avoid these undesirable minima several optimization algorithms, weight functions and thresholds were used. An initial optimization using a genetic algorithm provided a starting point, and reduced the size of the parameter space, for a Nelder-Mead simplex method algorithm to continue the optimization. If satisfactory results were not obtained, then the genetic solver was run

Table 2: Performance parameters for each polarization and frequency band. The subscripts on AR indicate transmission (t) or reflection (r). The requirements to be fulfilled in this work are IL and RL less than 0.5 dB and AR less than 0.78 dB.

	$17.7 - 20.2\,\mathrm{GHz}$	$27.5 - 30.0\,\mathrm{GHz}$
RHCP	RL & $\mathrm{AR_r}$	IL & $\mathrm{AR_t}$
LHCP	IL & $\mathrm{AR_t}$	RL & $\mathrm{AR_r}$

again with changed settings and/or updated penalty functions before moving on with the Nelder-Mead simplex algorithm. Likewise, if the results after this second optimization step were non-satisfactory the penalty function and parameters were tweaked and the Nelder Mead simplex algorithm was run again. The final algorithm used was a trust region method for when the minimum was in close proximity. The described procedure can be summarized by the flowchart illustrated in Figure 4. The utilized algorithms are all available in Computer Simulation Technology Microwaves Studio (CST MWS) as built-in optimization routines. Greater flexibility can be achieved in the optimization process if the simulation software is controlled externally by MATLAB. In this case a great number of optimization algorithms can be utilized.

A six layer CPSS design was optimized for normal incidence in CST MWS using a 32 GB RAM, Intel i7-2600 3.4 GHz CPU desktop computer, using the technique in Figure 4. A coarse simulation mesh of ten steps per wavelength was initially used in the genetic algorithm optimization in order to reduce the computation time of each iteration. Typically a few thousand iterations were carried out in this part of the procedure. The mesh settings were later gradually improved during the optimization cycles when the simplex algorithm and the trust region algorithm were employed, where roughly a few hundred iterations were carried out. A mesh convergence study was executed when a final design candidate fulfilling all requirements had been achieved. This study showed that the mesh settings used in the optimization routine were satisfactory, and that almost no noticeable improvement in accuracy was achieved if a mesh finer than 16 steps per wavelength was used.

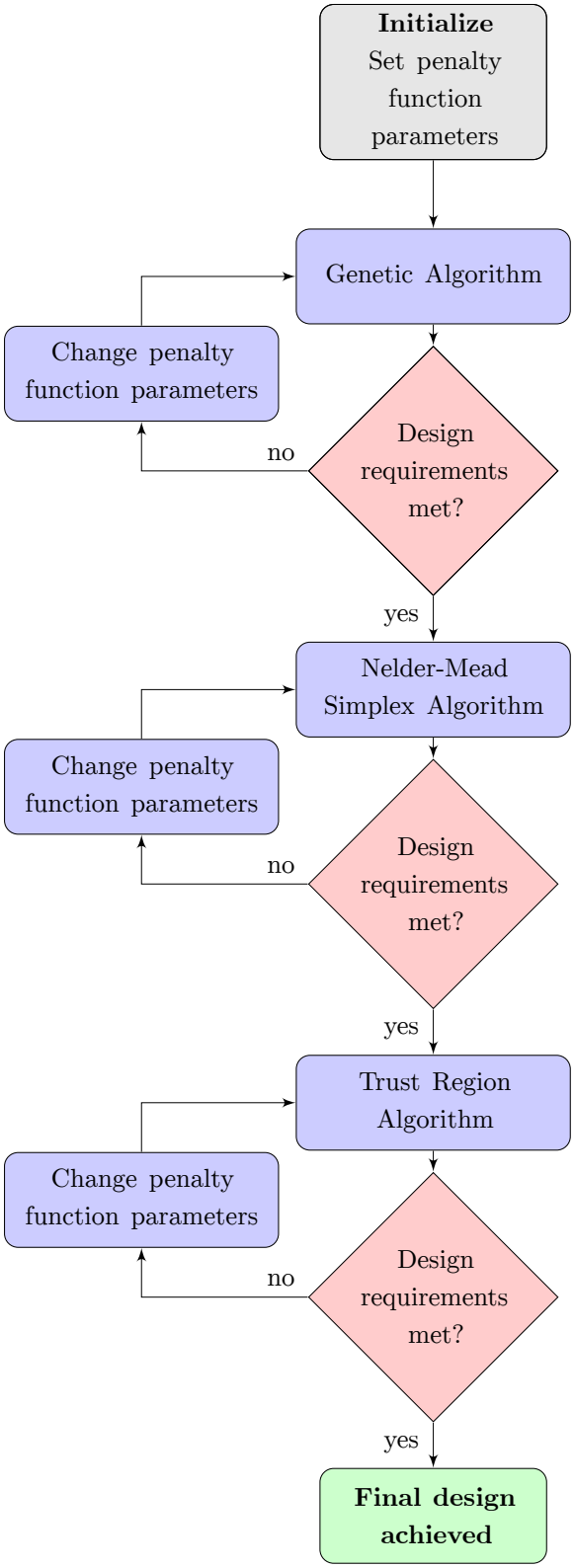

Figure 4: Flowchart for optimizing a dual band CPSS using built-in optimization algorithms in CST MWS.

Table 3: Material parameters of the meander line CPSS

Material	Rel. permittivity	Loss tangent	Thickness
Rohacell H31 spacers	1.043	0.002	d_1, d_2 and d_3
Arlon DiClad 880 substrates	2.17	0.003	0.127 mm
Copper, wires	$\sigma = 58\,\mathrm{MS/m}$		$18\,\mu$m
3M Scotch-Weld bonding layers	2.32	0.001	0.05 mm

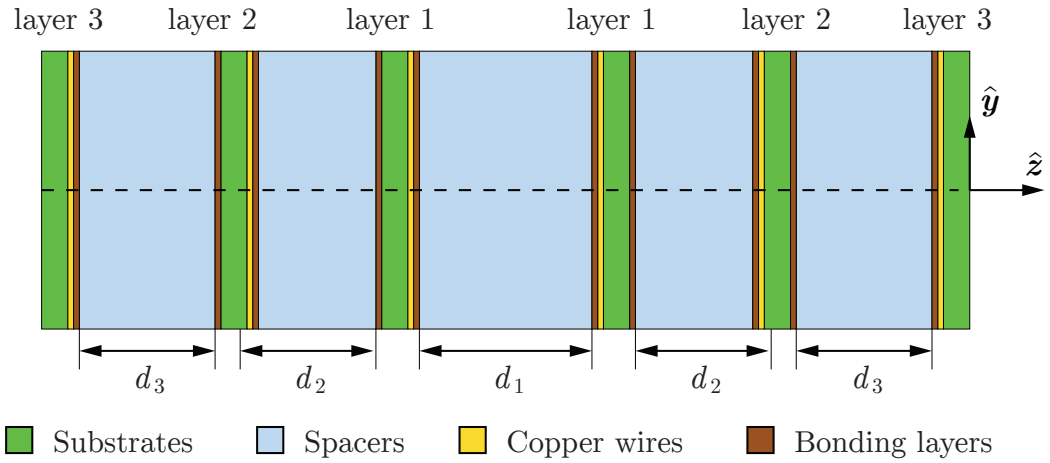

Figure 5: Side view of the dual band meander line CPSS consisting of six layers of substrates and five low permittivity spacers.

4 Simulated results

The optmized six layer CPSS, with 60° relative rotations between subsequent layers, consists of thin Arlon DiClad 880 teflon sheets with printed copper meander lines separated by low permittivity, low loss Rohacell HF31 spacers. The components of the structure were bonded together using thin bonding layers. The electrical properties and thickness of the bonding layers were estimated using the same procedure as in [5], where a similar CPSS was designed and fabricated. The material properties and the thickness of each layer of the dual band CPSS are presented in Table 3, and a side view of the CPSS can be seen in Figure 5.

The total thickness of the simulated design is 17.22 mm, which corresponds to 1.08 wavelengths at the center frequency of the lower band of operation $f = 18.95\,\mathrm{GHz}$. The meander lines of one unit cell as implemented in CST MWS can

Table 4: Design parameters of the dual band meander line CPSS.

Parameter	P	d_1	d_2	d_3	h_1
Value (mm)	5.49	3.80	2.90	3.24	1.14
Parameter	h_2	h_3	w_1	w_2	w_3
Value (mm)	1.21	1.25	0.99	0.61	0.12

be seen in Figure 6, and the values of the meander line thickness w_i and the meandering height h_i of each layer are given in Table 4. The side length of the unit cell P and the thickness of the spacers are also presented in Table 4. Only three different meander line layers and spacer thicknesses are present in the design due to the enforced symmetry introduced in Section 3.

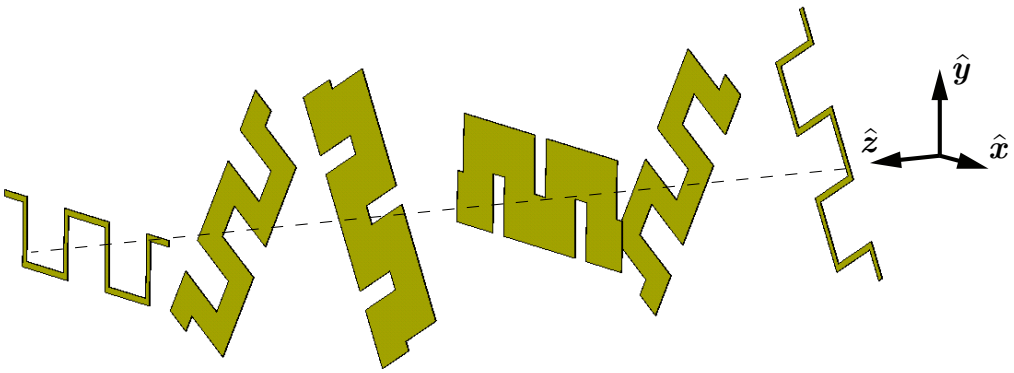

Figure 6: Meander lines of the six layers in the dual band CPSS design implemented in CST MWS. When a unit cell is defined, components extending outside of the unit cell are automatically pasted into the opposite side of the unit cell by the software.

Simulation results are presented in Figure 7 where 16 steps per wavelength mesh setting was used, and the IL, RL and AR for transmission and reflection are presented for both bands of operation. Red curves correspond to RHCP and blue curves to LHCP and it can be seen that the eight requirements specified in Table 2 are all fulfilled. When comparing the results in Figure 7 to the wideband meander line CPSS in [5] a substantial reduction in bandwidth can be observed in the dual band design. This is in part caused by the targeted dual band functionality as well as the relatively small frequency separation between the bands of operation.

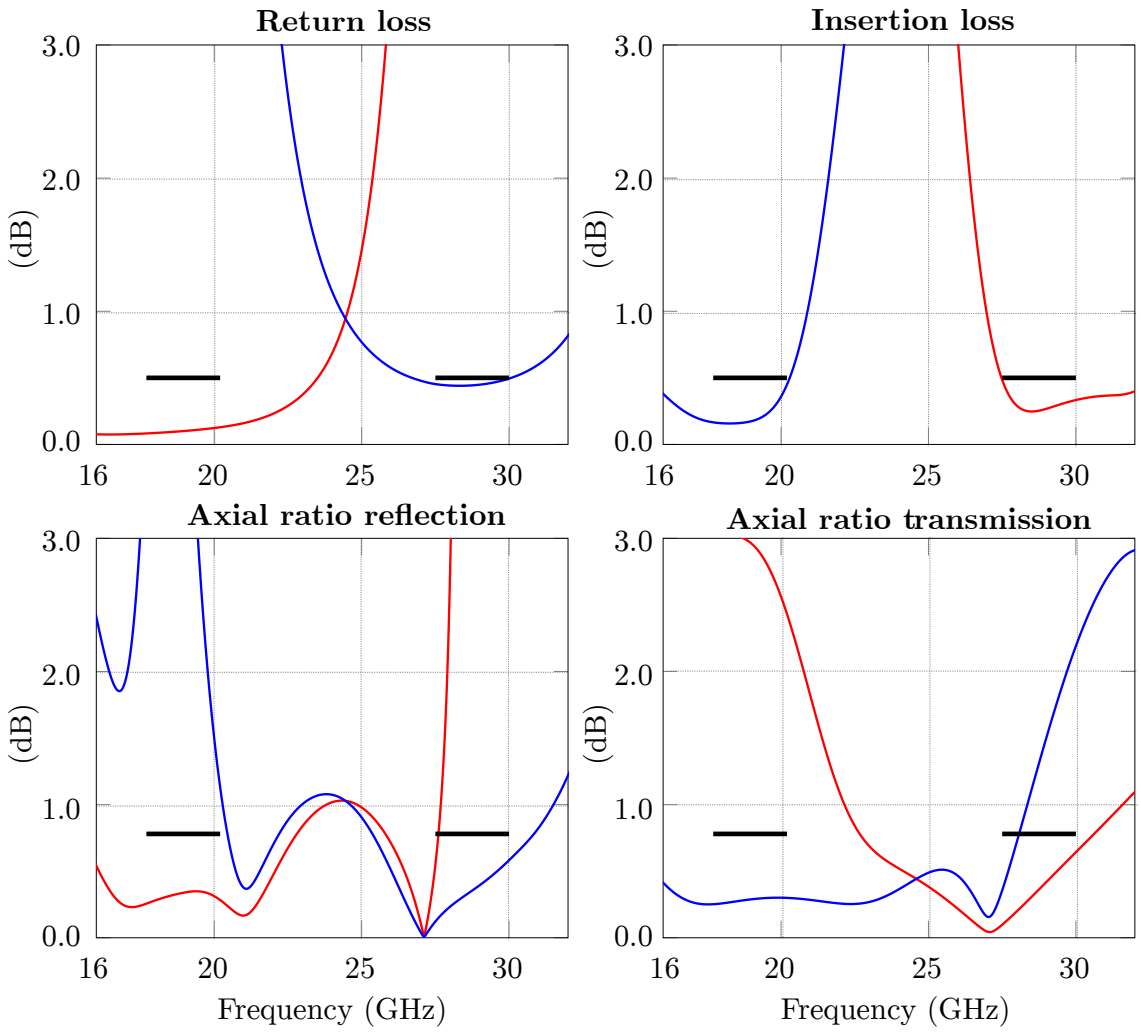

Figure 7: Simulated results of the meander line dual band CPSS, where red curves correspond to RHCP and blue curves to LHCP. The upper left plot shows the RL in both frequency bands and the lower left plot the corresponding AR. The upper right plot shows the IL in both frequency bands and the lower right plot the corresponding AR.

5 Prototype manufacturing and error estimates

A prototype of the optimized six layer dual band CPSS was manufactured and can be seen in Figure 8. The dimensions of the prototype are 310 mm × 310 mm and the total thickness is 17.11 mm, which should be compared to the thickness of the optimized simulated design of 17.22 mm. As was mentioned in Section 4, copper meander lines were printed on thin Arlon DiClad 880 substrates. The Rohacell HF31 spacers of custom thickness were manufactured by Evonik. The thickness of each spacer was measured individually, using a micrometer screw gauge, before assembling the prototype and it was concluded that the deviation between simulated and fabricated values was smaller than 0.1 mm. For the bonding layers a 3M Scotch-Weld 76 adhesive spray was used. Unfortunately, the actual thickness of the bonding layers proved difficult to estimate due to the Rohacell HF31 being porous and the adhesive penetrating the spacers in the process of assembly of the prototype.

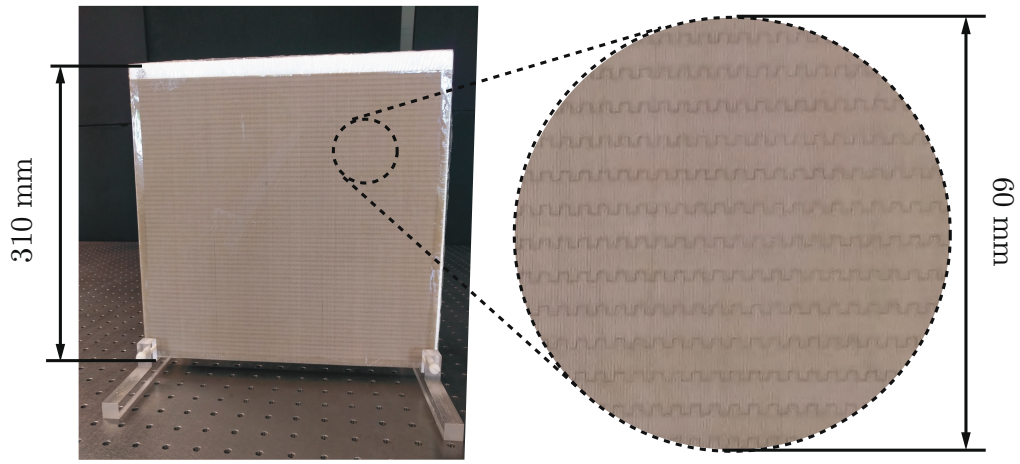

Figure 8: Manufactured dual band CPSS prototype.

In order to investigate the impact of the bonding layer thickness on the performance of the CPSS, a parametric study was carried out where the thickness of the bonding layers was varied, while the total thickness of the CPSS was kept fixed by compensating the thickness of the spacers by the same length. Simulated results are presented in Figure 9, where the solid, dashed, and dash-dotted curves correspond to the bonding layer thicknesses 0.05 mm, 0.12 mm and 0.19 mm, respectively. It can be seen that increasing the thickness of the bonding layers by a factor of two implies a negative frequency shift of about 0.7 GHz in RL and IL, as well as a detuning of the corresponding AR. Another source of error associated with the assembly of the prototype is the impact of a relative displacement in the xy-plane between subsequent layers in relation to the alignment in Figure 6. This effect was investigated by simulating the properties of the CPSS where translations in the horizontal and vertical directions were introduced using random shift variables, and where the

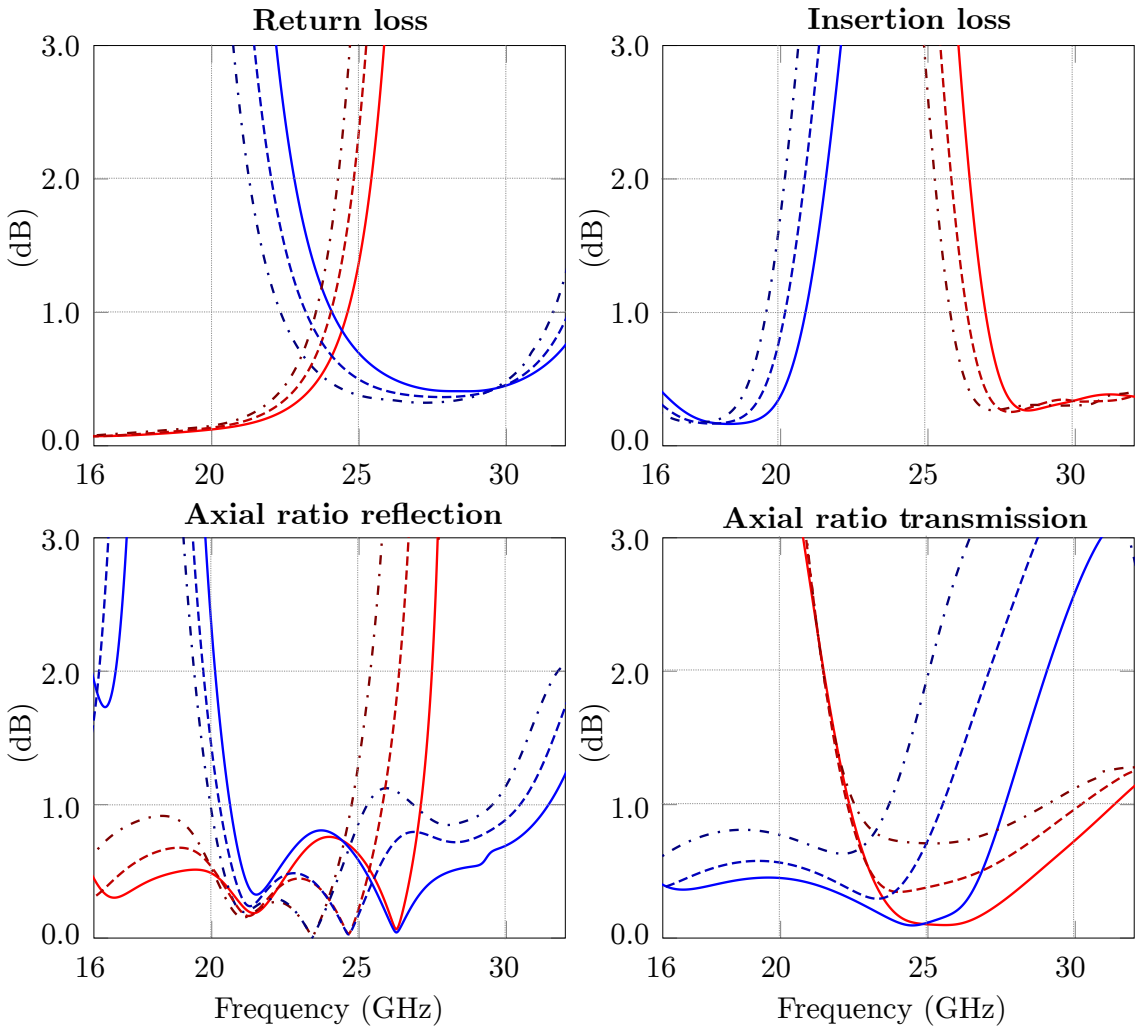

Figure 9: Parametric study of the thickness of the bonding layers in the meander line dual band CPSS. The upper left plot shows the RL in both frequency bands and the left plot the corresponding AR. The upper right plot shows the IL in both frequency bands and the lower right plot the corresponding AR. The solid, dashed, and dash-dotted curves correspond to the bonding layer thicknesses 0.05 mm, 0.12 mm and 0.19 mm, respectively.

maximum shift of each layer corresponded to a complete displacement in relation to the next layer. A total of 200 such simulations were carried out and the maximum deviation of the scattering parameters for each frequency are presented as colored bands in Figure 10. Here it can be seen that the impact of displacements of the layers in transverse directions is negligible in RL and IL, and on the order of 0.05 dB in AR. Similar results were presented in [23], where relative translations of subsequent layers of a multilayer CPSS in the optical regime were investigated.

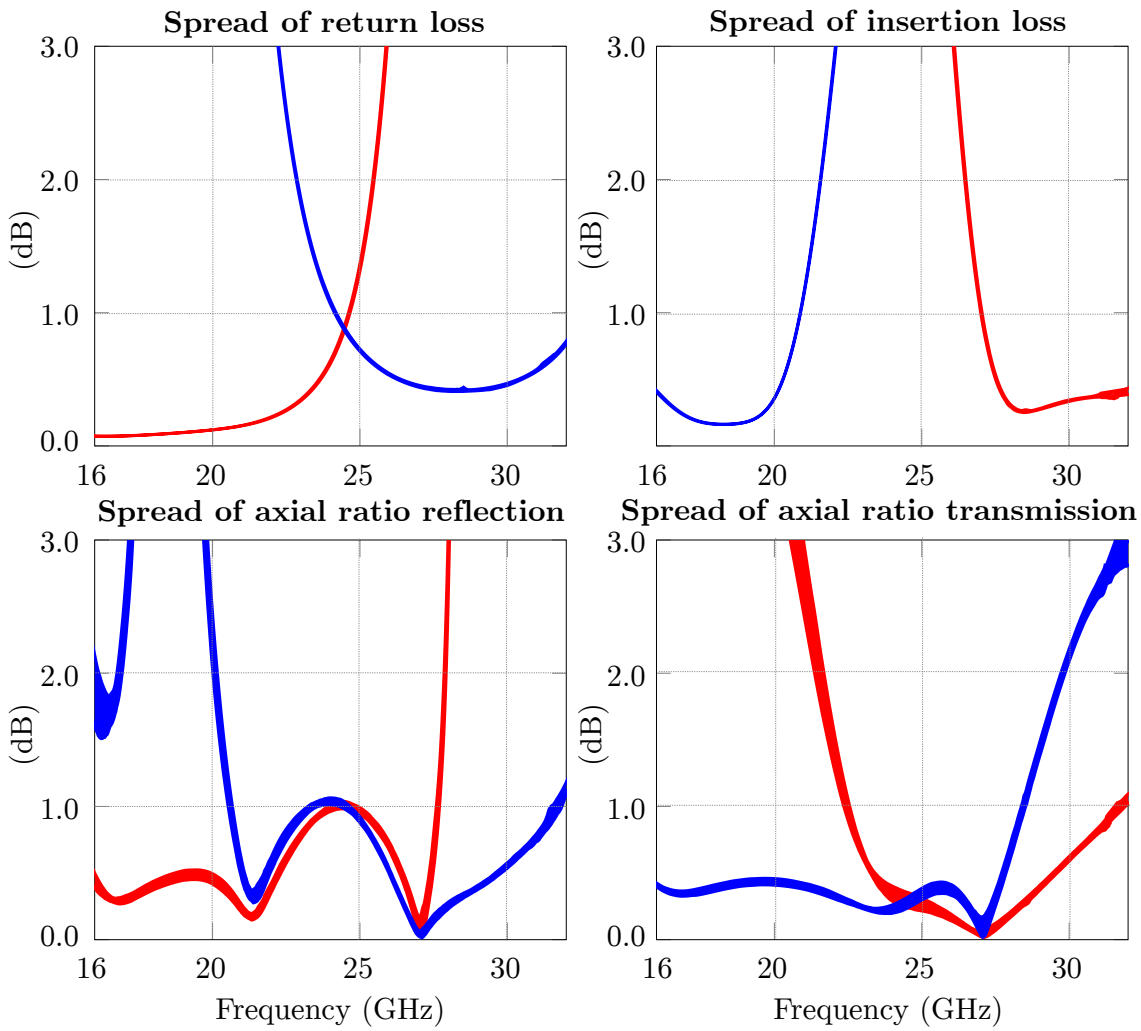

Figure 10: Simulations of relative translations of the layers of the CPSS. The maximum deviations of 200 simulations are shown.

6 Experimental setup and results

Experimental characterization of the transmission and reflection properties of the dual band CPSS prototype were carried out at Lund University. The frequency range $13 - 34\,\mathrm{GHz}$ was measured using two separate pairs of single-polarized, standard gain horn antennas. Two SATIMO SGH 1850 antennas were used to cover the lower frequency band, and two SATIMO SGH 2650 antennas were used for the upper frequency band. These antennas have a boresight cross-polarization discrimination better than 40 dB in their respective frequency range of interest. The experimental setup was assembled on a Newport RS2000 optical table, and the receiving and transmitting antennas were mounted on THORLABS PRMTZ8 motorized precision rotation stages. Two of such stages were used to control the yaw and the roll of each antenna, which in turn were connected to an Agilent E8364b vector network ana-

lyzer (VNA). The VNA and the rotational stages were controlled through MATLAB scripts using USB and GPIB to USB connections [9, 20]. The CPSS prototype was placed in a custom made sample holder of adjustable height made entirely of plastic and polymethyl methacrylate (PMMA). An overview of the experimental setup is presented in Figure 11.

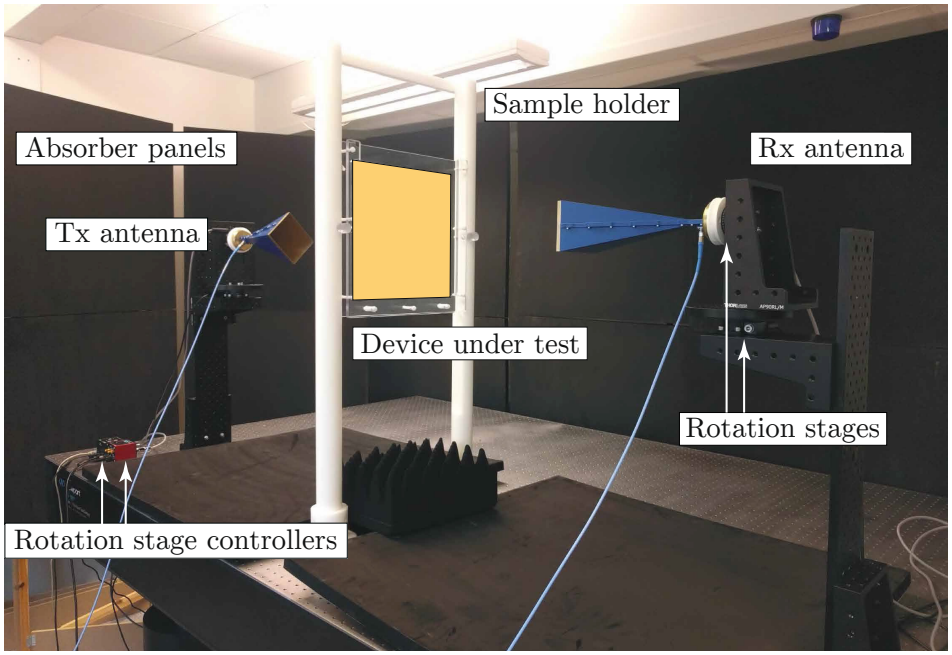

Figure 11: Experimental setup for dual/wide band characterization of a CPSS at frequencies 13-34 GHz .

The high degree of control in alignment of the setup provided by the optical table, the antenna fixtures and the rotational stages implied that the setup could easily be modified to measure at different distances between the sample and the antennas. An initial coarse alignment of all components of the setup was carried out using cross line lasers. After that, the alignment of the rotational stages were fine-tuned using feedback from the VNA. For the transmission measurements, a golden section search was utilized to maximize power throughput of the setup, given a fixed separation between the antennas, without the prototype present. In a similar way, alignment of the setup for reflection measurements used a golden section search maximizing reflection with the reference being an aluminum foil sheet water glued to the prototype [4]. This method achieved an accuracy in antenna rotation and jaw alignment on the order of 0.1°.

When the setup had been properly aligned, the scattering matrix components of interest in linear polarization were acquired and processed using the post processing method described in detail in[4], resulting in equivalent circular polarization scattering parameters of the device under test. When characterizing the transmission properties of the CPSS, the antennas were placed on each side of the prototype as in Figure 11. The scattering matrix components of the device under test were nor-

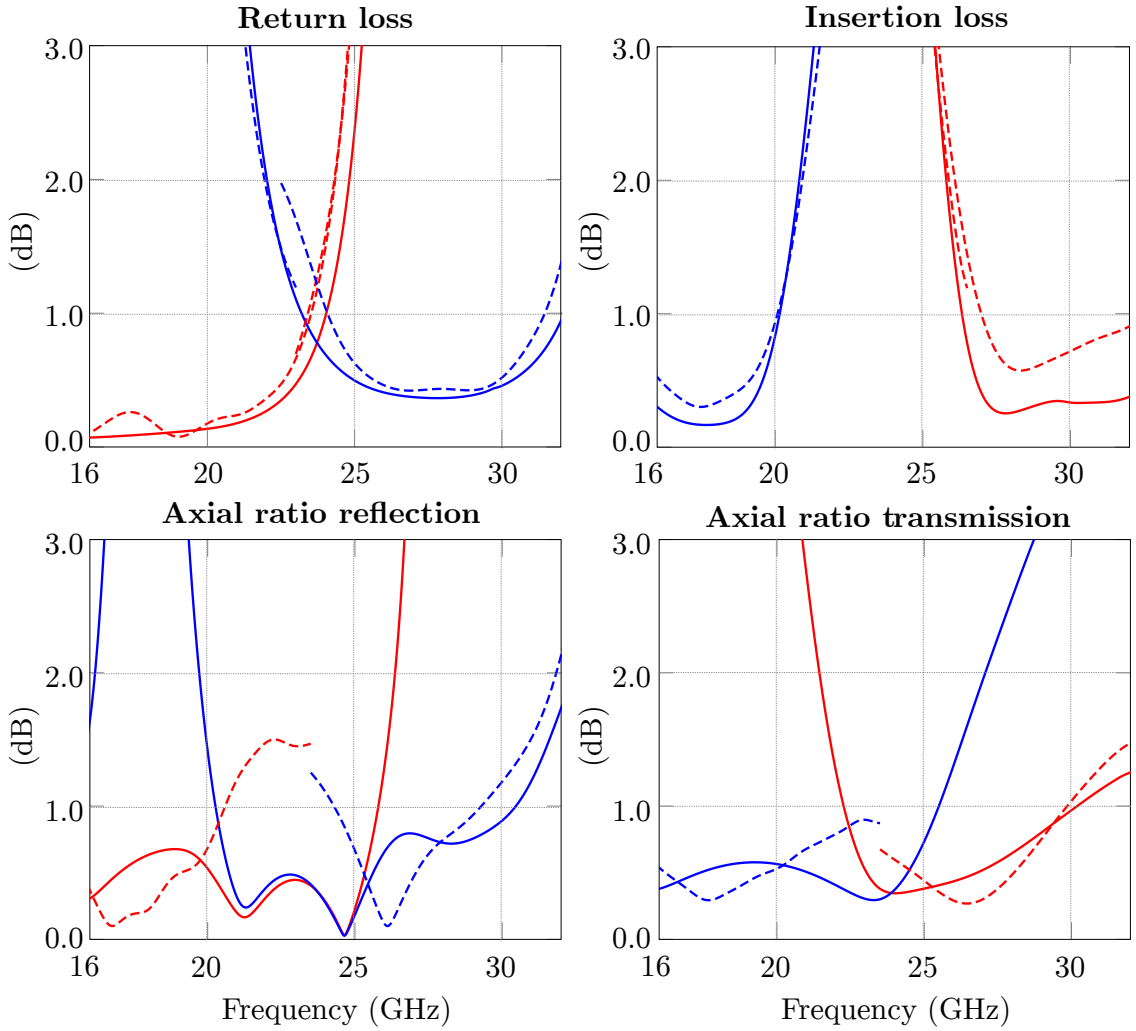

Figure 12: Experimental and simulated results of the meander line dual band CPSS. The upper left plot shows the RL in both frequency bands and the left plot the corresponding AR. The upper right plot shows the IL in both frequency bands and the lower right plot the corresponding AR. Experimental results are represented as dashed curves and simulated results as solid curves.

malized with a corresponding reference measurement, consisting of measurements of the empty setup. In reflection, both antennas were placed on one side of the device under test at an oblique angle of about 3°. This small incidence angle variation was simulated and it was concluded that the variations in the scattering parameters of the meander line CPSS were hardly noticeable. For the reference measurements in reflection, a thin aluminum foil was attached to the device under test using a small amount of water as an adhesive.

The characterized deviations between the optimized and fabricated designs due to manufacturing errors and uncertainties, discussed in Section 5, were used to generate an updated simulation model corresponding to the realized prototype. In

this design, the thickness of the spacers is $d_1 = 3.78\,\text{mm}$, $d_2 = 2.87\,\text{mm}$, $d_3 = 3.17\,\text{mm}$, and the updated bond layer thickness was set to 0.12 mm. A comparison between the updated simulation results and the experimental results are presented in Figure 12, were the dashed curves correspond to measurements and solid curves represent simulated results. It can be seen in the experimental data that two separate pairs of antennas were used to cover the full frequency range. The experimental AR curves are only plotted in the relevant regions of interest for each component, in order to make the figures more readable. Good agreement can be observed in general between the simulated and measured results. However, it can be noticed that the IL of the higher frequency band is about 0.2–0.3 dB larger than the simulated results. This is most likely caused by the fact that the material parameters used in the simulations are typically defined for frequencies less than 10 GHz. Both the Rohacell HF31 spacers and the adhesive layers most likely display increasing losses when higher frequencies are considered. When comparing the results in Figures 7 and 12 it is observed that the measured curves are shifted down in frequency of about 1.0 GHz in relation to the optimized simulation model. This is most likely caused by the additional thickness of the bonding layers, penetrating the Rohacell HF31 spacers.

7 Conclusions

A dual band circular polarization selective structure for K- and K_a-band applications has been presented. The structure consists of six cascaded layers of meander lines, separated by low permittivity spacers. Simulations of the design fulfill the strict design requirements of return loss and insertion loss better than 0.5 dB, and axial ratio better than 0.78 dB over the frequency bands 17.7–20.2 GHz and 27.5-30.0 GHz, with alternating circular polarizations in the two bands. A prototype was fabricated and characterized experimentally and good agreement has been observed between simulated and measured results. This type of cascaded circular polarization selective structures has been shown to possess great potential to achieve both wideband and multi-band filtering properties, and constitutes an interesting design concept for future ideas.

Acknowledgments

The authors of this paper kindly acknowledge Ron van Hoorn and Oliver Krause at Evonik for providing Rohacell HF31 samples for the manufacturing of the test panel. The Royal Physiographic Society of Lund is acknowledged for funding the experimental setup used in this work.

References

[1] S. M. A. M. H. Abadi and N. Behdad. "A broadband, circular-polarization selective surface". *Journal of Applied Physics* 119 (24) (2016): p. 244901.

[2] M. Albani, P. Balling, L. Datashvili, G Gerini, P. Ingvarson, K. Pontoppidan, M. Sabbadini, D. Sjöberg, S. Skokic, and G. Vecchi. "Concepts for polarising sheets & "dual-gridded" reflectors for circular polarisation". In: *ICECom Proceedings*. 2010, pp. 1–4.

[3] C. Cappellin, D. Sjöberg, A. Ericsson, P. Balling, G. Gerini, N. J. G. Fonseca, and P. D. Maagt. "Design and analysis of a reflector antenna system based on doubly curved circular polarization selective surfaces". In: *2016 10th European Conference on Antennas and Propagation (EuCAP)*. 2016, pp. 1–5.

[4] A. Ericsson, J. Lundgren, and D. Sjöberg. "Experimental characterization of circular polarization selective structures using linearly single-polarized antennas". *IEEE Trans. Antennas Propag.* 65 (8) (2017): pp. 4239 –4249.

[5] A. Ericsson and D. Sjöberg. "Design and analysis of a multilayer meander line circular polarization selective structure". *IEEE Trans. Antennas Propag.* 65 (8) (2017): pp. 4089–4101.

[6] *IEEE Standard Test Procedures for Antennas*. 2008.

[7] W. A. Imbriale, S. S. Gao, and L. Boccia, eds. "Space Antenna Handbook". Wiley, 2012.

[8] M Joyal and J Laurin. "Design and analysis of a cascade circular-polarization-selective surface at K band". *IEEE Trans. Antennas Propag.* 62 (6) (2014): pp. 3043–3052.

[9] *Keysight Instruments and MATLAB*. 2017.

[10] G. Kristensson. "Scattering of Electromagnetic Waves by Obstacles". SciTech Publishing, an imprint of the IET, 2016.

[11] J. Lundgren, A. Ericsson, and D. Sjöberg. "Design and Optimization of Dual Band Circular Polarization Selective Structures".

[12] J. Lundgren. "Dual Band Circular Polarization Selective Structures for Space Applications". MA thesis. Lund University, Department of Electrical and Information Technology, P.O. Box 118, SE-221 00 Lund, Sweden, 2016.

[13] G. A. Morin. "A simple circular polarization selective surface (CPSS)". In: *Antennas and Propagation Society International Symposium, 1990. AP-S. Merging Technologies for the 90's. Digest.* IEEE. 1990, pp. 100–103.

[14] R. Pierrot. *Reflector for circularly polarized waves*. 1970.

[15] S. Rao, L. Shafai, and S. K. Sharma. "Handbook of Reflector Antennas and Feed Systems Volume III: Applications of Reflectors". Artech house, 2013.

[16] D. Sjöberg and A. Ericsson. "A multi layer meander line circular polarization selective structure (MLML-CPSS)". In: *Proceedings of the 8th European Conference on Antennas and Propagation (EuCAP)*. IEEE. 2014, pp. 464–468.

[17] W. Tang, G. Goussetis, N. J. G. Fonseca, H. Legay, E. Sáenz, and P. de Maagt. "Coupled split-ring resonator circular polarization selective surface". *IEEE Trans. Antennas Propag.* 65 (9) (2017): pp. 4664–4675.

[18] W. Tang, S. Mercader-Pellicer, G. Goussetis, H. Legay, and N. J. G. Fonseca. "Low-profile compact dual-band unit cell for polarizing surfaces operating in orthogonal polarizations". *IEEE Trans. Antennas Propag.* 65 (3) (2017): pp. 1472–1477.

[19] I.-Y. Tarn and S.-J. Chung. "A new advance in circular polarization selective surface–A three layer CPSS without vertical conductive segments". *IEEE Trans. Antennas Propag.* 55 (2) (2007): pp. 460–467.

[20] *Thorlabs PRMTZ8 motorized precision rotation stage*. 2017.

[21] W. V. Tilston, T. Tralman, and S. M. Khanna. "A polarization selective surface for circular polarization". In: *Antennas and Propagation Society International Symposium, 1988. AP-S. Digest*. IEEE. 1988, pp. 762–765.

[22] J. Wang, Z. Shen, and W. Wu. "Broadband and high-efficiency circular polarizer based on planar-helix chiral metamaterials". *Applied Physics Letters* 111 (11) (2017): p. 113503.

[23] Y Zhao, M. Belkin, and A Alù. "Twisted optical metamaterials for planarized ultrathin broadband circular polarizers". *Nature Communications* 3 (2012): p. 870.